ELSEVIER

Mechanics of Materials 26 (1997) 35–42

MECHANICS OF MATERIALS

Rotating–bending fatigue of a TiNi shape-memory alloy wire

Hisaaki Tobushi [a,*], Takashi Hachisuka [a], Sinya Yamada [b], Ping-Hua Lin [c]

[a] *Department of Mechanical Engineering, Aichi Institute of Technology, 1247 Yachigusa, Yagusa-cho, Toyota 470-03, Japan*
[b] *Sato Kogyo, Ltd., Tokyo 103, Japan*
[c] *Department of Mechanical Engineering, Southeast University, Nanjing 210096, China*

Received 20 December 1996; revised 14 March 1997; accepted 21 March 1997

Abstract

The rotating–bending fatigue of a TiNi shape-memory alloy wire was investigated. The influence of air and water atmospheres, temperature, strain amplitude and rotational speed on the fatigue life was discussed. In the case of the strain amplitude due to the rhombohedral-phase transformation, the fatigue life lengthened above 10^7 cycles. In the case of the strain amplitude due to the martensitic transformation, the fatigue life in air was shorter than that in water. © 1997 Elsevier Science Ltd.

Keywords: Shape-memory alloy; Titanium–nickel alloy; Fatigue; Rotating–bending; Wire; Rotational speed; Atmosphere

1. Introduction

The shape-memory effect (SME) and the superelasticity (SE) appear in shape-memory alloys (SMA's). In TiNi SMA's, these properties occur due to the martensitic transformation (MT) and the rhombohedral-phase transformation (RPT). If SMA's are applied to the working elements of an actuator, a robot and a solid-state heat engine, SMA's perform cyclic motions. In order to evaluate the reliability of memory elements, cyclic deformation properties of SMA's must be established (Tobushi et al., 1991, 1996a,b). If we use SMA's under high cycles in actuators, robots and solid-state heat engines, the fatigue life of SMA's becomes an important problem in developing these devices (McNichols et al., 1981; Melton and Mercier, 1979; Miyazaki, 1990).

In SMA's, the fatigue limit of TiNi SMA's is high, because the grain size is small. Because the response property of SMA elements is determined based on the property of heat transfer, a thin wire is most widely used in applications. In a simple-pulley heat engine (Tobushi et al., 1990), an SMA element performs cyclic bending. In order to evaluate the fatigue property in these cases, it is necessary to carry out the rotating–bending test on the wire.

In the present study, a rotating–bending fatigue test machine for the SMA wire was developed. The influence of air and water atmospheres, strain amplitude, temperature and rotational speed on the fatigue of the TiNi SMA wire was investigated.

2. Experimental method

2.1. Material and specimen

Material was a Ti–55.3 wt% Ni SMA wire, 0.75 mm in diameter. A straight line was shape-mem-

* Corresponding author. Tel.: +81-565-488121; fax: +81-565-484555; e-mail: tobushi@me.aitech.ac.jp.

PII S0167-6636(97)00019-7

orized through shape-memory processing by keeping at 673 K for 1 h followed by cooling in a furnace. The grain size varied from submicron to several microns. The A_f point of a specimen determined by a tensile test was about 323 K. The length of the specimen was 155–255 mm. The distance between supports was 65–165 mm. The larger the curvature of the specimen, the shorter the distance between the supports.

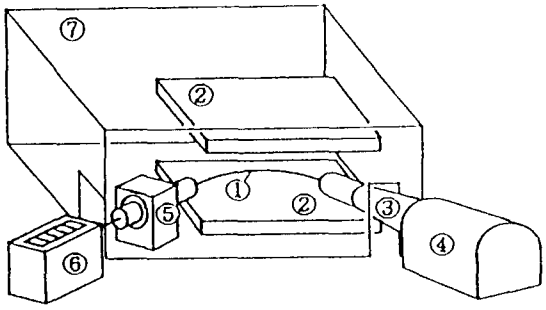

(a) Setup for the fatigue test in air

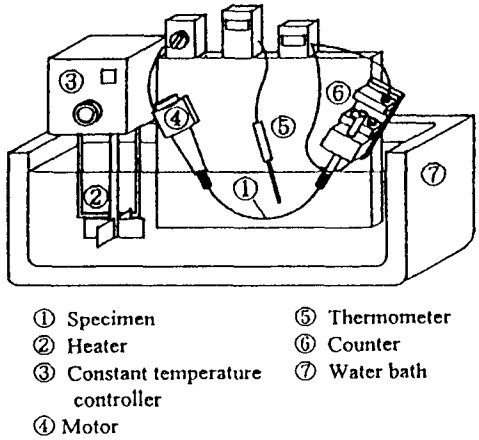

(b) Setup for the fatigue test in water

Fig. 1. Experimental apparatus. (a) Setup for the fatigue test in air. (b) Setup for the fatigue test in water.

2.2. Experimental apparatus

The experimental apparatus for the rotating–bending test of the wire is shown in Fig. 1. The apparatus was composed of a working part to perform the rotating–bending and a chamber or a water bath to keep the temperature constant. One end of the specimen was mounted to a motor and the other end rotated freely, at which the number of cycles to failure was measured. In order to avoid torsional moment, ball bearings were used at the supports of both ends. The specimen was in air or in water.

The curvature of the specimen was determined as follows. Before the test, the bent form of the specimen was traced on a section paper. After the test, the radius of curvature of a ruptured part was measured. Using the radius of curvature, the maximum strain on the surface of the specimen was obtained.

2.3. Experimental procedure

The rotating–bending test was performed in air and in water. In the experiment, the influence of air and water atmospheres, the maximum strain on the surface of the specimen (strain amplitude) ε_a, temperature T, and rotational speed n, on the fatigue was investigated. The strain amplitude was 0.5–2.5%. The temperature was room temperature (RT) in air, 303, 333 and 353 K. The rotational speed was 100–1000 rpm. In the case of RT in air, the temperature was not controlled.

In order to obtain the stress–strain relationship due to MT and RPT, the tensile test at various temperatures was carried out.

3. Experimental results and discussion

3.1. Deformation properties

The stress–strain curves obtained by the tensile test at various temperatures T are shown in Fig. 2. As seen in Fig. 2, in the case of $T = 303$ K below A_f, yielding due to RPT occurs under a stress of 50 MPa. The yielding due to RPT starts at a strain of 0.2% and is completed at 0.8%. After RPT, yielding due to MT occurs at a strain of 1.4% under a stress

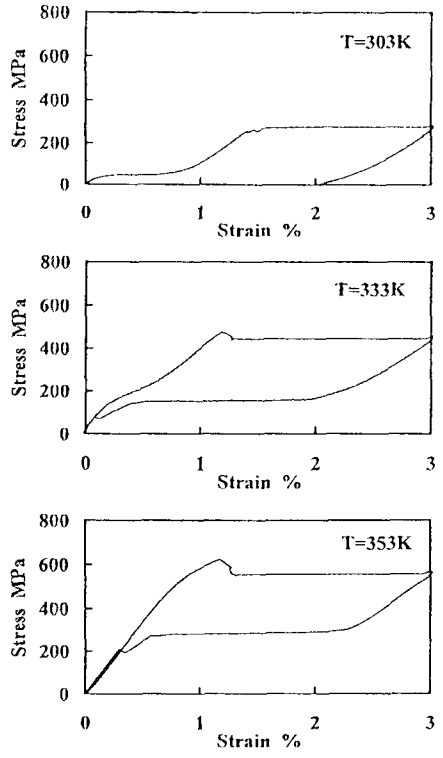

Fig. 2. Stress–strain curves.

of 250 MPa. In this case, residual strain appears after unloading. The residual strain disappears by heating above A_f under no stress. This phenomenon is the SME. In the case of $T = 333$ K and 353 K above A_f, yield stress due to both transformations increases in proportion to temperature. The reverse transformation occurs and strain is recovered during the unloading process. This phenomenon is SE. In the case of $T = 353$ K, RPT does not appear but only MT appears.

3.2. Stress distribution under bending

The stress distribution in a cross section and the transformed region in a longitudinal section of a wire which is subjected to bending are schematically shown in Fig. 3. The stress distribution and the transformed region are determined based on the deformation properties of the material shown in Fig. 2. As seen in Fig. 3, the central part is the elastic region and the transformed region expands from the surface area to the central part as the bending strain increases. In the surface area, RPT occurs at first and thereafter MT occurs as the curvature of bending increases. If the wire makes one revolution by keeping the bent form, the element in the surface area is subjected to tension and compression. Therefore, in the fatigue test, the element in the surface area is subjected to cyclic transformation due to tension and compression.

3.3. Temperature rise in air

The relationship between the temperature rise ΔT and time t obtained by the fatigue test at room temperature with various strain amplitudes, ε_a, under a constant rotational speed, $n = 300$ rpm, in air is shown in Fig. 4. As seen in Fig. 4, ΔT increases rapidly in the early cycles but reaches almost a constant value after 150 s. ΔT increases in proportion to ε_a. The relationship between the maximum saturated value ΔT_m and n is shown in Fig. 5. As seen in Fig. 5, the larger the n, the larger the ΔT_m. The dependence of ΔT_m on ε_a and n is explained as follows. As seen in Fig. 2, the stress–strain curve draws a hysteresis loop. The area surrounded by the hysteresis loop denotes dissipated strain energy per unit volume E_d. Based on E_d which appears in each cycle, the temperature rises. Because E_d is determined by the product of stress and strain, E_d increases in proportion to ε_a. If E_d is balanced with

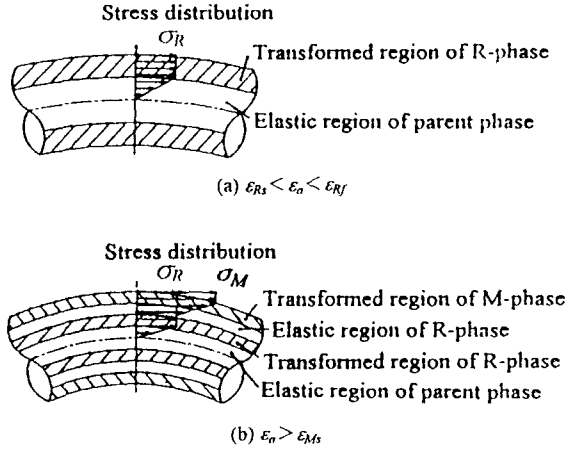

Fig. 3. Stress distribution and transformed region in the wire under bending. (a) $\varepsilon_{Rs} < \varepsilon_a < \varepsilon_{Rf}$. (b) $\varepsilon_a > \varepsilon_{Ms}$.

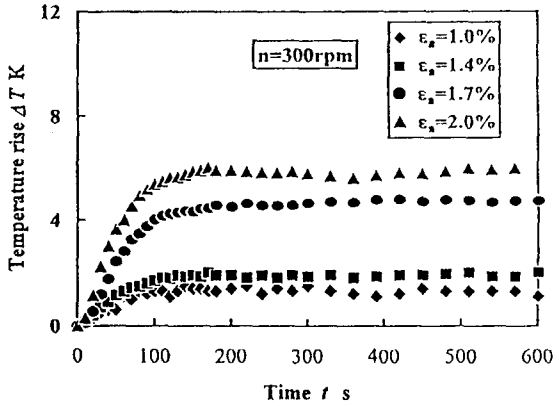

Fig. 4. Relationship between temperature rise ΔT and time t in air.

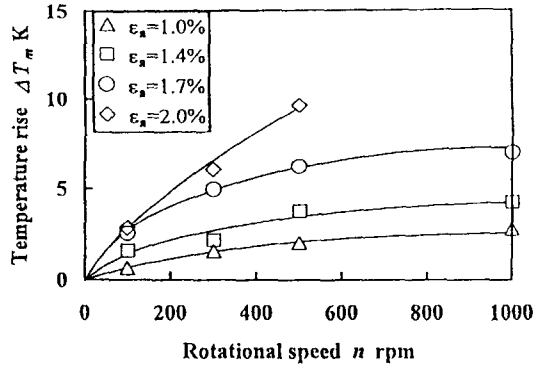

Fig. 5. Relationship between maximum temperature rise ΔT_m and rotational speed n.

heat conduction and radiant heat, ΔT is saturated to ΔT_m. If the strain rate is greater than 10%/min, the yield stress due to MT increases in proportion to the strain rate (Shaw and Kyriakides, 1995; Lin et al., 1996). Therefore, if n is large, E_d is large. Because ΔT increases as E_d increases, ΔT_m is large in proportion to n.

3.4. Fatigue properties

3.4.1. Fatigue in air

The relationship between the strain amplitude ε_a and the number of cycles to failure N_f, obtained by fatigue tests at various temperatures T under a constant rotational speed, $n = 500$ rpm, in air is shown in Fig. 6. In the case of $N_f = 10^6$ plotted with an arrow, the specimen was not ruptured. As seen in Fig. 6, in the case when ε_a is larger than 0.8%, N_f is small in proportion to ε_a. The relationship between ε_a and N_f in this region is expressed by a straight line. The slope of the straight line coincides at each temperature. If the straight line is expressed by the equation

$$\varepsilon_a = \alpha \cdot N_f^{-\beta}, \tag{1}$$

a value of β is 0.235. This value is smaller than $\beta = 0.5$ which is valid for normal metals. Eq. (1) corresponds to the Manson–Coffin relationship between the fatigue life and the total strain in low-cycle fatigue. The reason why β is small is explained as follows. As seen in Fig. 4, ΔT is large in proportion to ε_a. Yield stresses due to MT and RPT increase in proportion to temperature (Tanaka et al., 1986; Tobushi et al., 1995). Therefore, in the case of large ε_a, stress is high, resulting in a small N_f. As the result of small N_f for large ε_a, β is small.

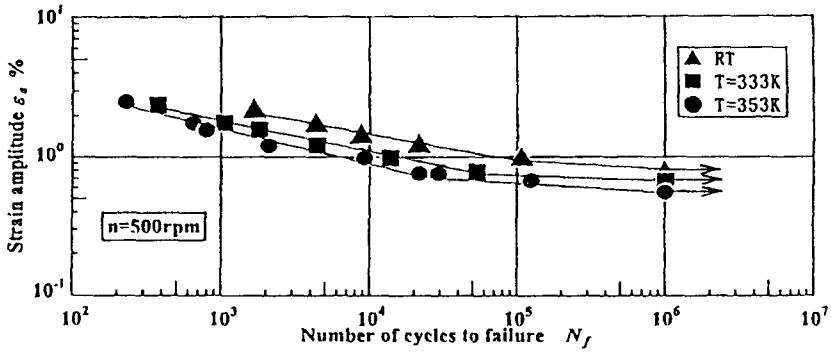

Fig. 6. Relationship between strain amplitude and the number of cycles to failure at various temperatures in air.

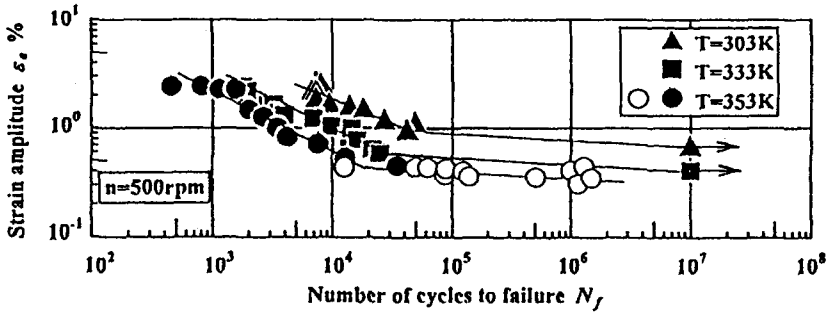

Fig. 7. Relationship between strain amplitude and the number of cycles to failure at various temperatures in water. ●, ■, ▲: Ruptures in the testing area; →: nondestructive; ○; nondestructive in the testing area but slipped or ruptured in the gripper.

In the region of $\varepsilon_a = 0.8–1\%$ or $N_f = 10^4–10^5$, the ε_a–N_f curve has a knee. In the case when ε_a is smaller than 0.8%, N_f increases significantly and the curve approaches a horizontal line. The region of ε_a, below 0.8% corresponds to RPT. Therefore, in applications of SMA's, the fatigue life is quite long if TiNi SMA is used in the region of the RPT.

If the temperature T is high, the curve moves to

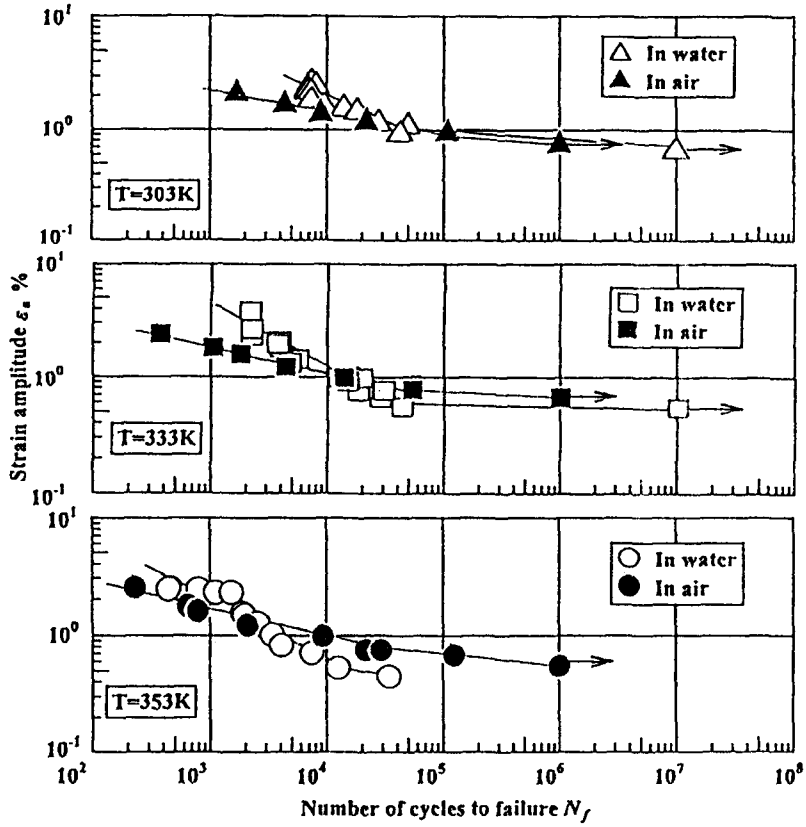

Fig. 8. Relationship between strain amplitude and the number of cycles to failure at various temperatures in air and in water.

the left and downward. That is, the higher the T, the smaller the N_f for the same ε_a. This is due to the fact that yield stresses due to MT and RPT are high in proportion to T, resulting in a small N_f.

3.4.2. Fatigue in water

The relationship between ε_a and N_f obtained by fatigue tests at various temperatures T under constant $n = 500$ rpm in water is shown in Fig. 7. As seen in Fig. 7, the overall inclination of the relationship is the same as that in air shown in Fig. 6. The slope of the curve represented by β in Eq. (1) in the region of large ε_a is 0.47. The value of $\beta = 0.47$ is larger than that in air, but is close to 0.5 which is valid for normal metals. In the case of fatigue tests in water, the temperature of the wire does not increase

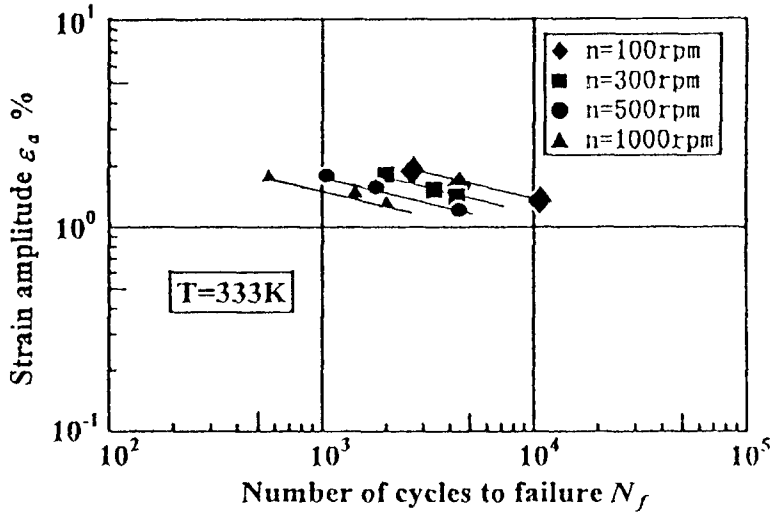

(a) In air

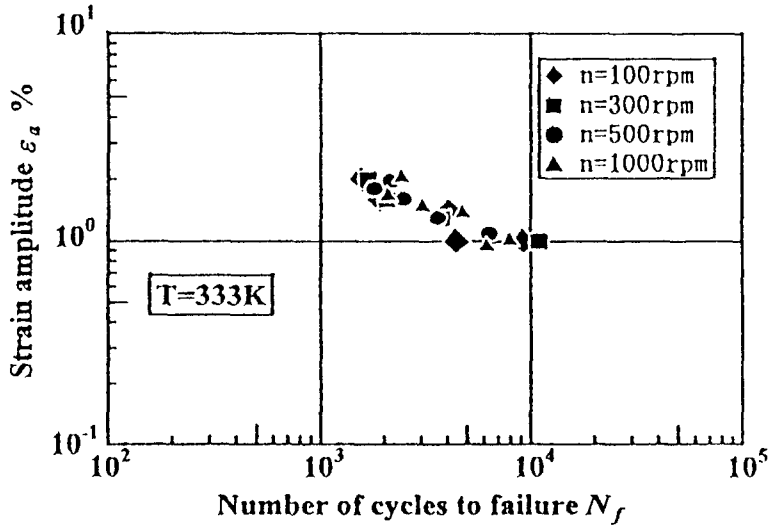

(b) In water

Fig. 9. Relationship between strain amplitude and the number of cycles to failure at various rotational speeds. (a) In air. (b) In water.

but is kept constant. Therefore the yield stress is constant during the fatigue test. In the case of normal metals in air, the yield stress and the plastic deformation properties do not change even if the temperature increases by 10K. Therefore the value of β is about 0.5 in the case of normal metals and TiNi SMA in water. As seen in Fig. 7, in the region of small ε_a, where RPT occurs, the fatigue life lengthens above 10^7 cycles.

3.4.3. Influence of air and water atmospheres

The relationship between ε_a and N_f obtained by fatigue tests at the same temperatures T in air and in water is shown in Fig. 8. As seen in Fig. 8, in the region of low-cycle fatigue below 10^4 cycles, N_f in air is small and the slope of the straight line β is small. As mentioned above, the transformation start line for MT is expressed (Tanaka et al., 1986) by

$$\sigma = C_M(T - M_s) \tag{2}$$

and that for RPT (Tobushi et al., 1995) by

$$\sigma = C_R(T - M_R), \tag{3}$$

where σ represents stress. M_s and M_R represent the transformation start temperatures of MT and RPT under no stress, respectively. C_M and C_R denote the slopes of the transformation start lines. For TiNi SMA, $C_M = 6$ MPa/K and $C_R = 15$ MPa/K. Therefore, if $\Delta T = 10$ K, the increase in MT stress is 60 MPa and that in RPT is 150 MPa. If the stress in the surface of a wire is high, the initiation of a fatigue crack is early, resulting in small N_f and small β in air. On the contrary, the temperature does not change in water. In the case of normal metals, even if the temperature rises by 10 K around room temperature, the yield stress and the plastic deformation property do not change as sensitively as SMA's. Therefore the value of β is about 0.5 for SMA in water and normal metals.

As seen in Fig. 8, the ε_a–N_f curves in air and in water intersect around the point of $\varepsilon_a = 1\%$. In the region of high-cycle fatigue above 10^5 cycles, the ε_a–N_f curves in air and in water approach horizontal lines. In the region of high-cycle fatigue, N_f in water is shorter than that in air. This may occur due to corrosion fatigue of the wire in water.

3.4.4. Influence of rotational speed

The relationship between ε_a and N_f obtained by fatigue tests at various rotational speeds n in air and in water is shown in Fig. 9. As seen in Fig. 9, in water, the data at various n lie on almost the same line. In air, the larger the n, the smaller the N_f. As observed in Fig. 5, if n is large, ΔT_m is large. Therefore, if n is large, the transformation stress is high, resulting in small N_f. In water, the temperature does not change even if n is different, resulting in the same N_f.

4. Conclusions

The rotating–bending fatigue test machine for the SMA wire was developed and the fatigue properties of the TiNi SMA wire were investigated. The results are summarized as follows.

(1) During the rotating–bending process in air, the temperature rises. The temperature rise is proportional to the strain amplitude and the rotational speed. The fatigue life shortens due to the temperature rise.

(2) If the strain amplitude is in the region of MT, the fatigue life in air is shorter than that in water.

(3) If the strain amplitude is in the region of RPT, the fatigue life lengthens above 10^7 cycles.

(4) The higher the temperature, the shorter the fatigue life.

Acknowledgements

The experimental work in this study was carried out with the assistance of the students of Aichi Institute of Technology, to whom the authors wish to express their gratitude. The authors also wish to express their gratitude to Professor K. Kimura and Professor H. Iwanaga for their support and to the Scientific Foundation of the Japanese Ministry of Education, Science and Culture for financial support.

References

Lin, P.H., Tobushi, H., Tanaka, K., Hattori, T., Ikai, A., 1996. Influence of strain rate on deformation properties of TiNi shape memory alloy. JSME Int. J. Ser. A 39 (1), 117–123.

McNichols, J.L. Jr., Brookes, P.C., Cory, J.S., 1981. NiTi fatigue behavior. J. Appl. Phys. 52 (12), 7442–7444.

Melton, K.N., Mercier, O., 1979. Fatigue of NiTi thermoelastic martensites. Acta Metall. 27, 137–144.

Miyazaki, S., 1990. In: Duerig, T.W., Melton, K.N., Stockel, D., Wayman, C.M. (Eds.), Thermal and Stress Cycling Effects and Fatigue Properties of Ni–Ti Alloys, Engineering Aspects of Shape Memory Alloys. Butterworth-Heineman, London, pp. 394–413.

Shaw, J.A., Kyriakides, S., 1995. Thermomechanical aspects of NiTi. J. Mech. Phys. Solids 43 (8), 1243–1281.

Tanaka, K., Kobayashi, S., Stato, Y., 1986. Thermomechanics of transformation pseudoelasticity and shape memory effect in alloys. Int. J. Plasticity 2, 59–72.

Tobushi, H., Ikai, A., Yamada, S., Tanaka, K., Lexcellent, C., 1996a. Thermomechanical properties of TiNi shape memory alloy. J. Phys. IV C1 (6), 385–393.

Tobushi, H., Iwanaga, H., Tanaka, K., Hori, T., Sawada, T., 1991. Deformation behavior of TiNi shape memory alloy subjected to variable stress and temperature. Continuum Mech. Thermodyn. 3, 79–93.

Tobushi, H., Kimura, K., Iwanaga, H., Cahoon, J.R., 1990. Basic research on shape memory alloy heat engine (output power characteristics and problems in development). JSME Int. J. Ser. I, 263–268.

Tobushi, H., Lin, P.H., Tanaka, K., Lexcellent, C., Ikai, A., 1995. Deformation properties of TiNi shape memory alloy. J. Phys. IV C2 (5), 409–413.

Tobushi, H., Yamada, S., Hachisuka, T., Ikai, A., Tanaka, K., 1996b. Thermomechanical properties due to martensitic and R-phase transformations of TiNi shape memory alloy subjected to cyclic loadings. Smart Mater. Struct. 5, 788–795.